Received: 28 February 2020 | Revised: 25 April 2020 | Accepted: 18 May 2020

DOI: 10.1002/amp2.10059

JOURNAL OF ADVANCED MANUFACTURING AND PROCESSING WILEY

RESEARCH ARTICLE

A high-efficiency novel IGCC-OTM carbon capture power plant design

Xiao-Yu Wu[1] | **Lili Cai**[2] | **Xuefeng Zhu**[2,3] | **Ahmed F. Ghoniem**[1] | **Weishen Yang**[2]

[1]Department of Mechanical Engineering, Massachusetts Institute of Technology, Cambridge, Massachusetts

[2]State Key Laboratory of Catalysis, Dalian Institute of Chemical Physics, Dalian, China

[3]Dalian National Laboratory for Clean Energy, Chinese Academy of Sciences, Dalian, China

Correspondence
Xuefeng Zhu, State Key Laboratory of Catalysis, Dalian Institute of Chemical Physics, Chinese Academy of Sciences, 457 Zhongshan Road, Dalian 116023, China.
Email: zhuxf@dicp.ac.cn

Present address
Xiao-Yu Wu, Department of Mechanical and Mechatronics Engineering, University of Waterloo, Waterloo, Waterloo

Funding information
Dalian National Laboratory for Clean Energy (DNL), Grant/Award Number: DNL180203; Exelon Corporation; Liaoning Revitalization Talents Program, Grant/Award Number: XLYC1801004; National Natural Science Foundation of China, Grant/Award Number: 21776267; Youth Innovation Promotion Association of the Chinese Academy of Sciences

Abstract

Coal power plants play an important role in supplying affordable and reliable electricity. It is necessary to develop high-efficiency and low-cost carbon capture (CC) technologies to mitigate the associated global warming. Using H_2S-tolerant oxygen transport membranes (OTMs) for hydrogen production and CO_2 separation can significantly reduce the energy penalty of CC in integrated gasification combined cycle (IGCC) power plants. We carried out system-level analysis to investigate a novel IGCC-CC power plant design using OTMs. We studied the impacts of various operating parameters on the overall efficiency and energy penalty. This novel IGCC-OTM system has an overall efficiency 3.2%-point lower than the same system without CC, much lower than the IGCC with water-gas shift reactors and acid gas removal units (IGCC-WGS) of 6.8%-point drop. The specific primary energy consumption for CO_2 avoided (SPECCA) of this novel technology is 1.08 MJ $kgCO_2^{-1}$, which is 59.4% lower than that of the IGCC-WGS.

KEYWORDS

carbon capture (CC), hydrogen production, IGCC, minimal energy consumption, oxygen transport membrane (OTM)

1 | INTRODUCTION

Coal power plants continue to play an important role in supplying affordable and reliable electricity in developing countries, especially in South and Southeast Asia (even though they are being closed in the developed countries in Europe and Northern America due to the climate policies).[1] Moreover, fossil fuels power plants can maintain the energy security of the grid and have positive impacts on the labor market.[2,3] Implementing cleaner coal power plants with carbon capture (CC) in the developing world can promote energy equity and security,[4] which addresses the sustainable development goals (SDGs) set by the United Nations such as

Xiao-Yu Wu and Lili Cai contributed equally to this work.

affordable and clean energy, and climate action goals.[5]

The integrated gasification combined cycle (IGCC) with precombustion CC is a promising technology to implement CC in fossil fuel power plants.[6,7] However, the energy penalty associated with CC generally leads to an efficiency reduction of 7% to 12% points.[7-9] The specific primary energy consumption for CO_2 avoided (SPECCA) can be as high as 2 to 4 MJ $kgCO_2^{-1}$.[10,11] The costs of CO_2 avoided were estimated to be \$30 to 86/ton CO_2,[12,13] which will increase the electricity production costs if CC is implemented. The total investments of IGCC-CC plants were estimated to be \$2513 to 4451/kW, with the cost of energy \$65.9 to 151.4/kWh.[13] The energy penalty and increase in capital and operational costs make CC less favorable unless high carbon taxes were introduced. New systems should be developed to decrease the CO_2 avoided energy consumption and costs in IGCC plants.

The conventional IGCC-CC process uses water-gas shift (WGS) reactors to convert the gasification products to higher concentration of H_2 and CO_2. Next CO_2 is separated and captured, typically using physical solvents such as Selexol and Rectisol.[14] The auxiliary power consumption of the cycle accounts for as high as 18.6% of the overall power output when 98% of the CO_2 is captured, around half of the auxiliary power for CC.[9] In addition, the air separation unit (ASU) also accounts for a large amount of the auxiliary power consumption in the IGCC-CC cycles.[15] Several membrane reactors, such as the Pd membrane[16] and metal-organic frameworks membrane[17] reactors have been developed to reduce the energy consumption associated with CO_2 capture. In the case of Pd membranes, the energy penalty is around 7% to 8% with SPECCA of 2.5 to 3.6 MJ $kgCO_2^{-1}$ due to the additional step of H_2S separation and the exergy loss resulting from quenching the gasifier products to 400 to 500°C for the stable operation of Pd membranes.[16 New membranes for hydrogen production such as the oxygen transport membranes (OTMs) are being developed to tolerate H_2S and operate at higher temperatures closer to 1300°C to avoid quenching.[18,19]

OTMs work at elevated temperatures of 700 to 1600°C,[20-22] and hydrogen production from water splitting in OTMs has previously been investigated.[23,24] Water splitting occurs on the high oxygen partial pressure side of the OTM reactor to produce hydrogen, while the oxygen permeates through the membrane to the other side due to the potential gradient across the membrane. To increase the gradient to enhance oxygen permeation and water splitting, a low-quality fuel such as syngas can be used to react with the permeated oxygen.[24] Recently, our groups developed a robust H_2S tolerant OTM reactor for hydrogen separation, which demonstrates the potential of integrating OTMs in an IGCC-CC process.[18] Figure 1 shows the operation of OTM in this process. Coal gasification products are fed on side I and undergo full oxidation with the permeated oxygen from the water splitting reaction on side II. The oxygen permeation is in the form of oxygen ions, associated with electrons or holes to maintain the neutrality of the bulk membrane. The overall reaction in the OTM reactor is the weakly exothermic WGS reaction, as the hydrogen oxidation on side I and water splitting on side II cancel out with thermal and species balanced by the oxygen flux (shown in Figure 1). We fabricated membranes of 75 wt% $Sm_{0.15}Ce_{0.85}O_{2-\delta}$ - 25 wt% $Sm_{0.6}Sr_{0.4}Cr_{0.3}Fe_{0.7}O_{3-\delta}$ (SDC-SSCF) for this application, while non-precious metal catalysts, 10 wt% Ni/ SDC were applied on the membrane surfaces to enhance surface reactions. Experimental results showed that this novel OTM reactor maintained high and stable performances (9 mL cm^{-2} min^{-1} [STP] ≈ 6.70 μmol cm^{-2} s^{-1}) under reducing gas environment mimicking the gasification products from a coal-slurry fed general electric energy (GEE) gasifier with H_2S concentrations as high as 1000 ppm.[18] Meanwhile, efforts from various companies and institutes such as Praxair and the Institut für Keramische Technologien und Systeme (IKTS) Fraunhofer have been carried out to commercialize OTM reactors for various applications, such as oxygen generation and syngas production.[25] OTMs have been proposed to replace the cryogenic ASU, and system analysis showed that the former can decreases the energy consumption for oxygen production, compared with the latter when the heat recovery rate is higher than 92%.[26] However, it has been shown that when OTM is used to replace the ASU in IGCC, the efficiency increase is only about 1% point because the H_2S and CO_2 purification is still needed.[15]

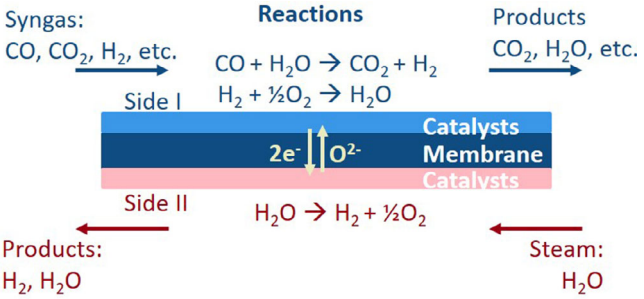

FIGURE 1 Schematic shows the operation of an oxygen transport membrane (OTM) in the IGCC-CC process. On side I, coal gasification products undergo full oxidation with the oxygen permeated across the membrane. The oxygen source is the water splitting reaction on side II, producing hydrogen and oxygen. Oxygen permeation in an OTM is in the form of oxygen ions, associated with electrons or holes, which is driven by chemical potential gradient across the membrane

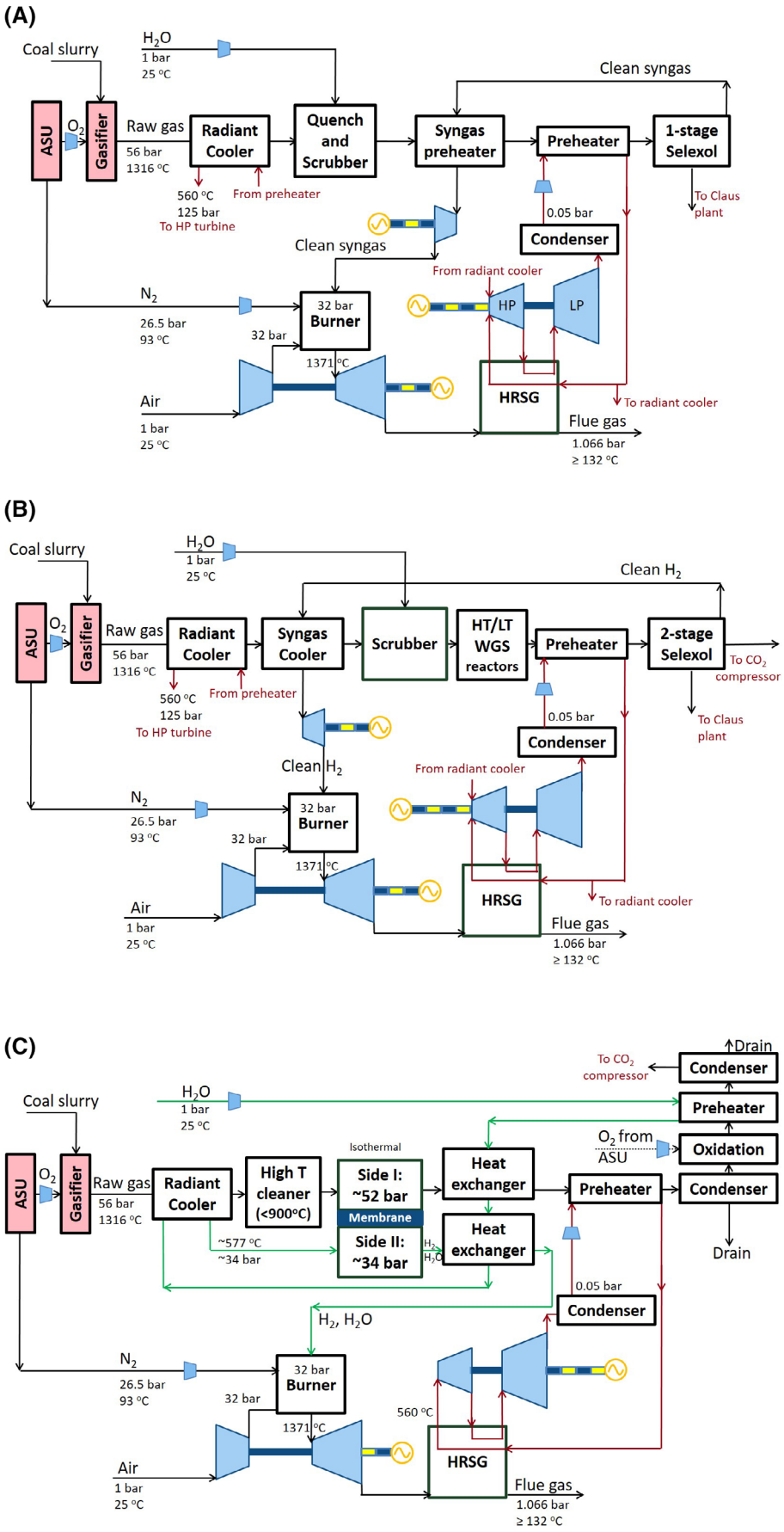

FIGURE 2 Schematics of the three IGCC processes modeled in this study. A, IGCC without CC (IGCC-REF), B, IGCC with two WGS reactors and two-stage Selexol process for acid gas removal (IGCC-WGS) to achieved 97% carbon capture, and C, IGCC with membrane reactor for hydrogen separation, CO_2 removal and sulfur production (IGCC-OTM). The gas turbine inlet temperature TIT for all systems is 1371°C (F class turbines). The gasifier is not modeled in our study, but the auxiliary power consumption of the gasifier is scaled with coal input.[28] Conventional cryogenic ASU is used to produce pure O_2 for gasification and burning unconverted fuel on side I of the OTM reactor

In this article, we study a novel integration of OTM in the IGCC process (IGCC-OTM), where an OTM reactor is used to replace the WGS reactors, the CO_2 and H_2S removal processes in order to achieve higher efficiency for power generation. We first compare the first law efficiency, auxiliary energy consumptions and SPECCA among three IGCC processes: IGCC without CC as a reference (IGCC-REF, Figure 2A), IGCC with CC consisting of two WGS reactors and a two-stage Selexol acid gas removal system (97% CO_2 removal, IGCC-WGS, Figure 2B), and IGCC with OTM noted as IGCC-OTM (Figure 2C). Next the impact of different operating parameters, such as the gas conversion, temperature, and pressure drop on the performance of the IGCC-OTM process is investigated.

2 | PROCESS LAYOUTS AND ASSUMPTIONS

2.1 | General assumptions and inputs

System level models were developed in Aspen Plus to compare the CC energy penalty in the two different IGCC processes, that is, IGCC-WGS and IGCC-OTM. The Peng-Robinson-Boston-Mathias (PR-BM) equation-of-state method was used to evaluate the thermodynamic properties at high pressure operations, which has been verified in previous IGCC system simulations.[27] The flowsheets and configurations of the Aspen models of all the cycles in this article can be found in Supporting Information. The simulation results of the IGCC-REF were validated against a study of a similar system[28] as shown later in the article.

TABLE 1 Raw gas species mole fraction from a GEE gasifier[28]

Species	Mole fraction (−)
Ar	0.0086
CH_4	0.0012
CO	0.3579
CO_2	0.1366
COS	0.0002
H_2	0.3416
H_2O	0.1358
HCl	0.0008
H_2S	0.0073
N_2	0.0080
NH_3	0.0021

Conventional natural gas-fired turbines cannot work with hydrogen rich fuels, and hydrogen turbines are under development.[29] Gas turbines fueled with high concentration of hydrogen up to ~97.5% by volume are being tested in pilot plants.[30] The hydrogen turbines used in the IGCC-WGS and IGCC-OTM systems were assumed to be equivalent to a natural gas-fired *F* class gas turbine, and the gas turbine inlet temperature (TIT) is around 1400°C.[31] In this study, we fixed the TIT to be 1371°C, the same as the IGCC reference case[28] for a fair comparison. Diluents in the combustor are the high pressure N_2 from the air separation unit in the gasifier and excess air. The ratio of the molar flow rates of the nitrogen diluent and the raw gas is 0.873:1 for IGCC-REF and IGCC-WGS, which depends on the oxygen consumption in the gasifier.[28] If the nitrogen is not enough to keep the adiabatic flame temperature of the mixtures below 1371°C, excess air is fed into the combustor. For IGCC-OTM, extra diluents are available, such as the nitrogen due to the use of an oxy-fuel oxidizer and unconverted steam. In these systems, the combustor is modeled as an adiabatic equilibrium reactor. The flue gas temperature at the outlet of the heat recovery steam generator (HRSG) in the steam cycle is set above 132°C, and the actual outlet temperature depends on the constraint of the minimum internal temperature approach (MITA) in the HRSG.

Previous studies show the potential of integrating coal gasification with solid oxide fuel cells (SOFC) for high efficiency power generation with CC.[32,33] However, the power output per SOFC stack is in the range of 1 to 2000 kW.[33] For large power plants of 500 to 1000 MW outputs, combined cycles are more favorable. In this article, the power plant is designed to be 1000 MW, and therefore, we only consider systems with combined cycles.

The GEE gasification technology[28] is used for all the IGCC systems. The gasifier operates at 1316°C and 5.6 MPa with a coal-water slurry fed system; the dry solids concentration of the final slurry is about 63%. The coal to water ratio is 1:0.41 by mass, and no extra steam is fed along with the oxygen in the gasifier. High-volatile A bituminous coal (Illinois No. 6) is used for the analysis. The higher heating value (HHV) of the as-received coal is 27.135 MJ kg^{-1}. The auxiliary loads for the gasifier include the energy consumption for coal handling, coal milling, sour water recycle slurry pump, slag handling, ASU auxiliaries, and the compressors of air, nitrogen, and oxygen. The sum of the auxiliary loads is assumed to scale with the coal input linearly and is calculated from the results in previous studies.[28]

In the system model, inputs are the high temperature raw gas from the coal gasifier (1316°C and 5.6 MPa), the

TABLE 2 Modeling assumptions

Fuel	
Coal rank	High-volatile A bituminous (Illinois No. 6) HHV (as-received) = 27.135 MJ kg^{-1}
Gasifier	
Technology	GEE gasification technology
Operating temperature (°C)	1316
Operating pressure (MPa)	5.6
Syngas composition	Shown in Table 1
Combustor	
Combustor is modeled as an adiabatic equilibrium reactor by minimizing the Gibbs free energy	
Water-gas shift reactor	
Each WGS reactor is modeled as a stoichiometric reactor with 84% CO conversion to achieve 97% CO final conversion[28]	
Gas turbine	
TIT[a] (°C)	1371
Diluents	Compressed N_2 from the air separation unit, excess air, and/or unconverted steam
Combustor pressure (MPa)	3.2
Isentropic efficiency (%)	85
Compressor (air or N_2)	
Isentropic efficiency (%)	84
Heat exchangers	
Minimum internal temperature approach (MITA) (°C)	20 Heat recovery steam generators (HRSG): 10°C
Pressure drop (%)	5
Steam cycle	
TIT (°C)	560
HP turbine inlet pressure (MPa)	12.5
HP turbine outlet pressure (MPa)	0.568
Turbine efficiencies (%)	90
Pump efficiency (%)	75
Flue gas outlet temperature (°C)	132 (or higher due to the constraint of MITA in HRSG)
Condenser outlet temperature (°C)	25
Selexol process	
Work consumption	Calculated from Equation (1)
CO_2 removal efficiency (%)	90
H_2S removal efficiency (%)	99.6
H_2 recovery efficiency (%)	99.4
High temperature gas cleaning	
Operating temperature (°C)	~900°C
Membrane reactor	
Operating temperature (°C)	850°C
Syngas conversion on side I (%)	99[b]
Water conversion on side II (%)	54[b]
Reactor design	See Figure 3A

(Continues)

TABLE 2 (Continued)

CO_2 compressor	
CO_2 delivery pressure (MPa)	12
Exit CO_2 stream composition (mol%)	>99% CO_2 (EOR ready)
Isentropic efficiency (%)	84
Intercooler temperature (°C)	25

[a]TIT, turbine inlet temperature.
[b]The conversion ratios are selected based on the thermodynamic equilibrium calculation as show in Figure 3B,C.

high pressure nitrogen from the ASU in the gasifier (93°C and 2.65 MPa), and air and water from the atmospheric condition (25°C and 0.1 MPa). The raw gas species from the gasifier are summarized in Table 1. Minor species, that is, Ar, N_2, COS, HCl, and NH_3, are neglected as they contribute little to the heating value for efficiency calculation. The raw gas is quenched to different temperatures in a radiant syngas cooler and a high pressure hot steam is generated. As shown in Figure 1, in the IGCC-REF and IGCC-WGS, the hot steam (560°C and 12.5 MPa) is used in the steam cycle, while in the IGCC-OTM, the hot steam (~577°C and 3.4 MPa) is used for hydrogen production in the membrane reactor.

The layouts for the three IGCC systems are shown in Figure 2, and the base conditions for the three IGCC systems are summarized in Table 2. The assumptions for conventional components such as water pump, gas compressor, combustors are consistent with the literature.[28] The flowsheets can be found in Supporting Information (Figures S1-S7). Since the WGS reactors and the OTM reactor operate at different temperature ranges, that is, 250 to 450°C and 700 to 1600°C, respectively, the reactor integrations are different for the IGCC-WGS and IGCC-OTM systems, which will be described in the following sections.

2.2 | IGCC-WGS

In the IGCC-WGS system (Figure 2B), the raw gas from the radiant syngas cooler is further cooled down, first by the cool syngas from the Selexol process and then by a water scrubber (quenching) to a temperature around 216°C, making it ready for the low temperature dust removal. After gas cleaning, the cooled raw gas with excessive amount of water is fed into the high temperature and then low temperature WGS reactors to convert CO and H_2O into CO_2 and H_2, with 97% CO conversion (Each WGS reactor is hence modeled as a stoichiometric reactor with 84% CO conversion).[28] The water flow rate is determined so that the steam-to-dry gas molar ratio is 0.3 at the outlet of the shift reactor.[28] The product from the WGS reactor then undergoes a two-stage Selexol process for H_2S and CO_2 removal. The syngas (now rich in H_2) is preheated and expanded to the operating pressure of the combustor, that is, 3.2 MPa.

The 2-stage Selexol process is applied in the IGCC-WGS system to remove H_2S and CO_2: the captured H_2S goes through a Claus process to produce sulfur, while CO_2 is captured, compressed and stored.[34] The inlet gas temperature of Selexol process is at ambient temperature, and the power consumption is obtained using a fitted function in turns of the CO_2 flow rate in the flue gas entering the Selexol process:[28]

$$W_{\text{selexol}} = 1.679 \times \dot{Q}_{CO_2} \quad (1)$$

where W_{selexol} is the power consumed in the Selexol process, (kW_e), and $\dot{Q}_{CO_2}$ is the CO_2 flow rate in the flue gas, (kmol h^{-1}). The Selexol process is designed to capture 97% of the CO_2 at most, with tail gas recycling,[28] and the outlet of the separated CO_2 from the process is at 2.1 MPa, which has to be compressed to higher pressure, that is, 12 MPa to be captured or used in enhanced oil recovery (EOR) process.

2.3 | IGCC-OTM

In the IGCC-OTM system (Figure 2C), the H_2S-resistant OTM reactor replaces the WGS reactors, acid gas removal and CC units. In addition, the OTM operating at elevated temperatures, for example, 700 to 1000°C, can be thermally integrated with the high temperature system for better energy efficiency. High temperature dust removal systems which operates around 900°C are installed downstream of the gasifier to filter the dust in the gas.[35] After cleaning, the syngas is fed into the low oxygen partial pressure side (side I) of the membrane reactor, while the steam fed on the high oxygen partial pressure side (side II). As the steam concentration is low in the gasification products, no further processing is needed before entering the OTMs. On the catalytic membrane surface, water

splits into hydrogen and oxygen ions. The hydrogen, being diluted with the unconverted water, serves as the fuel in the gas turbine cycle, while the oxygen ions diffuse across the membrane to side I and oxidize the syngas into H_2O and CO_2 on that side. At the same time, H_2S on side I is also oxidized to SO_2, and is converted to sulfur via the Claus reaction.[36-38] After that, the steam is condensed, the solid sulfur is separated, and CO_2 is captured and compressed. One such SDC-SSCF OTM has been experimentally demonstrated for stable hydrogen production in high H_2S concentration environments.[18]

The overall reaction in the OTM reactor is the weakly exothermic WGS reaction (shown in Figure 1). The input feed gas, that is, water, is preheated to a temperature slightly lower than the operating temperature, keeping the operation of the OTM reactor isothermal. In order to estimate the gas conversion ratios on both sides I and II in the base case, we use thermodynamic equilibrium conditions, in other words the maximum conversions that can be achieved with infinite membrane surfaces, which has been used in the literature to estimate the membrane performance in the best scenarios.[21] A rate-base model for the membrane reactor can give more details about the conversion ratios with a specific membrane reactor design and membrane surfaces.[39,40] In Section 5.1, we will present the impacts of gas conversion ratios on the IGCC-OTM system efficiency if the thermodynamic equilibrium conditions are not achievable.

In an OTM reactor, the oxygen permeation is driven by the oxygen chemical potential gradient across the membrane. Therefore, if the gradient is maintained, there will be finite oxygen flux across the membrane and hence, oxidation and splitting reactions occur on sides I and II, respectively.[39] Countercurrent design, shown in Figure 3A, can maintain the gradients on both ends with high conversions. Here, we calculate the oxygen partial pressure under equilibrium conditions at the two ends as a function of the conversion ratios at 850°C, using Cantera.[41] GRI-Mech 3.0 mechanism[42] was implemented to calculate the gas phase thermodynamic equilibrium. For each end of the membrane, we fixed the gas inlet conditions on one side and varied the gas conversion ratios on the other side to compare the corresponding oxygen partial pressures under thermodynamic equilibrium conditions. The results are shown in Figure 3B,C, and the gas inlet conditions are summarized in Table 3. When the conversion ratios on sides I and II are ~100% and 54.5%, respectively, finite oxygen partial pressure gradients across the membrane can be maintained under thermodynamic equilibrium. Therefore, the base case conversion ratios were assumed to be: on the syngas side, syngas conversion is 99%, and on the hydrogen production side, water side conversion is 54%. Later in Section 5.1, we will show how the system efficiency will change when the gas conversions are lower than the thermodynamic equilibrium conditions.

Downstream of the OTM reactor, the hydrogen and unconverted steam on side II are further diluted by the nitrogen from the ASU and excess air to limit the TIT to 1371°C, similar to the IGCC-WGS. On side I, the products go through a solid filtration system and then a condenser. Next, the unconverted CO and H_2 react with pure oxygen from the ASU in a catalytic oxidization reactor and form CO_2 and H_2O, respectively. High purity CO_2 can be obtained by feeding the products through another condenser. The energy consumption for the filtration system is ignored. Yet 5% pressure drop is assumed in the condenser and heat exchangers.

One energy penalty in the membrane reactor is the pressure drop and compensation, which leads to higher pump and compressor power consumption. In this article, we analyzed the pressure drop in a simplified monolith membrane reactor based on the correlation for a fully developed channel flow. For other membrane reactor designs, higher fidelity models should be developed to study the dependence of the pressure drop on the reactor design and operating conditions. Detailed discussions will be given in the following sections.

3 | EFFICIENCY DEFINITION AND MODEL VALIDATION

The first law efficiency of the IGCC systems is defined as

$$\eta_{\mathrm{IGCC}} = \frac{W_{\mathrm{net}}}{HHV_{\mathrm{coal}}} \tag{2}$$

where W_{net} is the network of the system, (W). The network is calculated as,

$$W_{\mathrm{net}} = W_{\mathrm{GT}} + W_{\mathrm{ST}} + W_{\mathrm{EXP}} + \left(\sum W_{\mathrm{pump}} + \sum W_{\mathrm{CO_2}} + \sum W_{\mathrm{O_2}} + W_{\mathrm{Selexel}} + W_{\mathrm{aux-gasifier}} + W_{\mathrm{BOP}} + W_{\mathrm{transformer}}\right) \tag{3}$$

where W_{GT}, W_{ST}, and W_{EXP} are the work produced by the gas and steam turbines and the syngas expander, respectively, (W). The auxiliary power consumptions (negative values, see Table 4) are $\sum W_{\mathrm{pump}}$, $\sum W_{\mathrm{CO_2}}$, $W_{\mathrm{O_2}}$, W_{Selexol}, $W_{\mathrm{aux\text{-}gasifier}}$, W_{BOP}, and $W_{\mathrm{transformer}}$ (W), which correspond to the water pump work, the compression work for the captured CO_2 and the oxygen for oxidation, the power consumption for the Selexol process, the auxiliary loads for the gasifier, the balance of the plant, and the transformer losses, respectively.

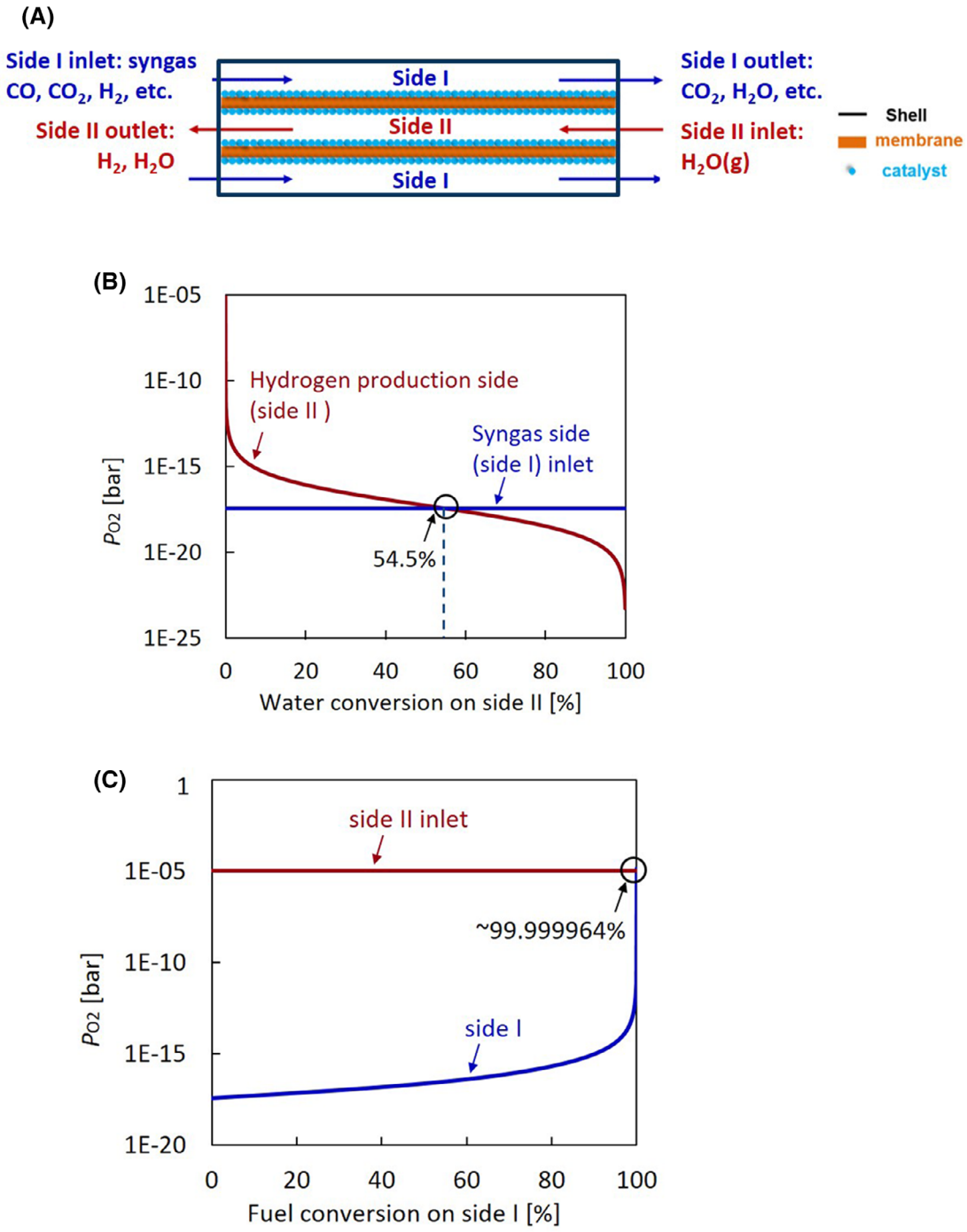

FIGURE 3 Schematic graphs of A, the membrane reactor in a countercurrent tubular configuration, with catalysts decorating the membrane walls. The dependence of oxygen partial pressures at the equilibrium conditions on the conversion ratios of B, water, and C, syngas on side II and I, respectively, at 850°C

The auxiliary loads of the gasifier and the balance of the plant are estimated to be linearly scaled with the coal input, while the transformer loss is scaled with the sum of the auxiliary loads of the plant. The balance of the plant includes the energy consumption of the circulating water pump, ground water pumps, cooling tower fans, Claus plant auxiliaries and the recycle compressor (if exists). In IGCC-OTM process, the oxygen stream for oxidation of the unconverted syngas is supplied by the same ASU used to supply O_2 to the gasifier, although the pressure in the oxidizer is slightly lower. The auxiliary work for the gasifier is then scaled with the amount of oxygen required for the entire system, as oxygen generation is the major part of the auxiliary power consumption in the gasifier.

The system model for the IGCC-REF (an F class gas turbine TIT = 1371°C, and the overall coal HHV

input = 1 596 183 kW) is validated against a previous detailed study.[28] The power output and efficiency are compared in Figure 4. In our model, the syngas inlet temperature to the gas turbine cycle is slightly higher, and the heat recovery for the steam cycle is slightly lower, due to the system model simplification. This results in higher gas turbine output and lower steam turbine output. Our simplified system shows good agreement with the detailed model, with 1.6% points difference as shown in Figure 4B.

TABLE 3 The inlet conditions for the oxygen partial pressure calculations

Name	Values
Side I: syngas side pressure (MPa)[a]	5.2
Side II: water side pressure (MPa)	3.4
Side I inlet composition[b]	Molar fraction (dimensionless)
CH_4	0.0012
H_2	0.3416
CO	0.3579
H_2O	0.1358
CO_2	0.1366
N_2	0.0269
Side II inlet composition	Molar fraction (dimensionless)
H_2O	1.0

[a]The pressures on the sides I and II are average values.
[b]Side I inlet composition is derived from the raw gas composition in Table 1. N_2 is used to model other minor species, for example, Ar, COS, HCl, and NH_3.

4 | COMPARISONS BETWEEN THE IGCC SYSTEMS UNDER BASE CASE CONDITIONS

The assumptions for all the cycle components are summarized in Table 2. Simulation results are summarized in Table 4. The work outputs and the combined cycle auxiliary loads (absolute values) are shown in Figure 5. The IGCC-REF has the largest work output and the smallest auxiliary loads, while the IGCC-WGS shows the opposite trend. The auxiliary power consumption for the CC in the IGCC-OTM (ie, water pump, acid gas removal, O_2, and CO_2 compressors) is 81% lower than that of the IGCC-WGS. For the same coal input, the IGCC-OTM produces 12% higher net work than the IGCC-WGS.

CO_2 emission for the three systems are shown in Figure 5C. The IGCC-OTM achieves almost 100% CC while the IGCC-WGS captures around 97% of the CO_2 produced. Even though IGCC-OTM captures more CO_2 than IGCC-WGS, the former outperforms the latter by 3.6% points in efficiency. And the IGCC-OTM has an efficiency only 3.2% point lower than the IGCC-REF without CC.

TABLE 4 Simulation results of the three IGCC systems with input of 1000 MW

	Conventional IGCC without carbon capture	Conventional IGCC with 97% carbon capture	Novel IGCC with oxygen transporting membrane
Notation	IGCC-REF	IGCC-WGS	IGCC-OTM
Gas turbine cycle network (MW)	304.0	282.9	316.8
Steam turbine cycle network (MW)	139.6	112.9	105.0
Expander work (MW)	5.0	4.5	0.0
Reactant compressor/pump work (MW)	−0.13[a]	−0.29	−0.57
O_2 compressor work (MW)	0.00	0.00	−0.023
Selexol process work (MW)	−1.56	−11.6	0.00
CO_2 compressor work (MW)	0.00	−6.69	−2.97
Aux-gasifier (MW)	−64.10	−64.10	−65.10
BOP (MW)	−7.60	−9.70	−9.70
Transformer (MW)	−1.55	−1.96	−1.66
IGCC cycle network (MW)	373.6	305.9	341.8
IGCC efficiency (%)	37.4	30.6	34.2
SPECCA (MJ kg CO_2^{-1})	/	2.66	1.08

Note: The gas turbine inlet temperatures (TIT) for all the cycles are kept at 1371°C.
[a]Negative values mean power consumption.

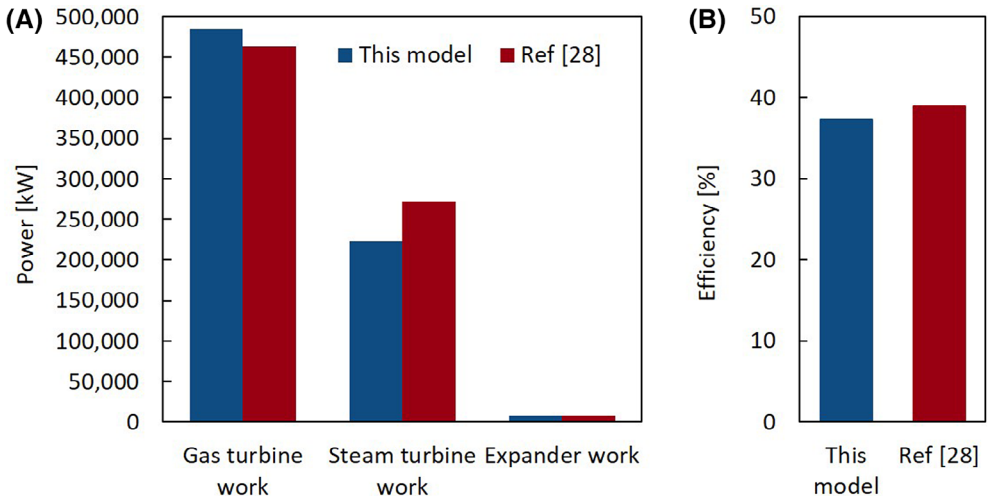

FIGURE 4 Comparisons of A, power outputs and B, efficiency of IGCC-REF between our model and a previous detailed study[28]

In addition, the specific primary energy consumption for CO_2 avoided (SPECCA) of the IGCC-OTM is only 1.08 MJ $kgCO_2^{-1}$, which is 59% lower than that of the IGCC-WGS (2.66 MJ $kgCO_2^{-1}$). Thus, the penalty for CC is decreased in the IGCC-OTM, making the energy-related operation cost of the IGCC with CC more economic. In the following section, the sensitivity of the IGCC-OTM system efficiency to the OTM operating temperatures and pressure drops, and the conversion ratios of water and syngas will be discussed.

5 | IMPACTS OF THE OPERATING CONDITIONS

5.1 | Conversion ratios of water and raw gases

In the base case, the raw gas and water conversion ratios on sides I and II are assumed to be 99% and 54%, respectively, according to the thermodynamic equilibrium calculation in Figure 3B,C. However, these high conversion ratios could result in an impractically long membrane reactor and impact the pressure drop in the reactor. In this section, we study the sensitivity of the system efficiency to the conversion ratios on sides I and II. Results are shown in Figure 6.

For side I raw gas conversion, Figure 6A shows that when the ratio decreases from 99% to 88%, the efficiency drops from 34.2% to 30.5%. Therefore, high syngas oxidation ratios is an important specification for the membrane reactor to have the IGCC-OTM system more efficient than the IGCC-WGS. The oxygen consumption increases in the catalytic oxidation reactor to oxidize more unconverted fuel, which increases the power consumption in air separation in the gasifier. In addition, the amount of hydrogen produced from water equals to the amount of fuels oxidized in the raw gas. Lower raw gas conversion leads to less hydrogen delivered to the combined cycle, and reducing the network output in the combined cycle. Furthermore, when the syngas conversion drops to 90%, the gas turbine TIT cannot reach 1371°C (Figure 6A) due to the excess nitrogen from the oxidizer and the unconverted steam. This leads to further efficiency decrease.

For side II, the water conversion ratio has very small impact on the overall efficiency when it changes from 54% to 48.5%, as shown in Figure 6B. The raw gas flow rate and its conversion ratio are both fixed on side I, and hence, the amount of hydrogen produced from water is constant. Lower water conversion ratio leads to higher water diluent on side I, and less compressed air is needed to control the TIT. However, when water conversion is below 48%, there is too much water diluent on that side and the TIT could not reach 1371°C. Hence, it is important to keep the water conversion above 48% when designing the membrane reactor.

5.2 | Membrane temperature dependence

The impact of membrane operating temperatures on the IGCC-OTM system efficiency is shown in Figure 7A. The maximum conversion ratios of raw gas on side I and H_2O on side II are estimated using thermodynamic equilibrium conditions as described in Section 2.3 and Figure 3. The maximum values for syngas conversion ratio are higher than 99%, so the ratio of 99% is assumed for all the temperatures. Yet the H_2O conversion ratio increases with temperatures as shown in Figure 7B, and the corresponding values are chosen for each temperature in the system analysis.

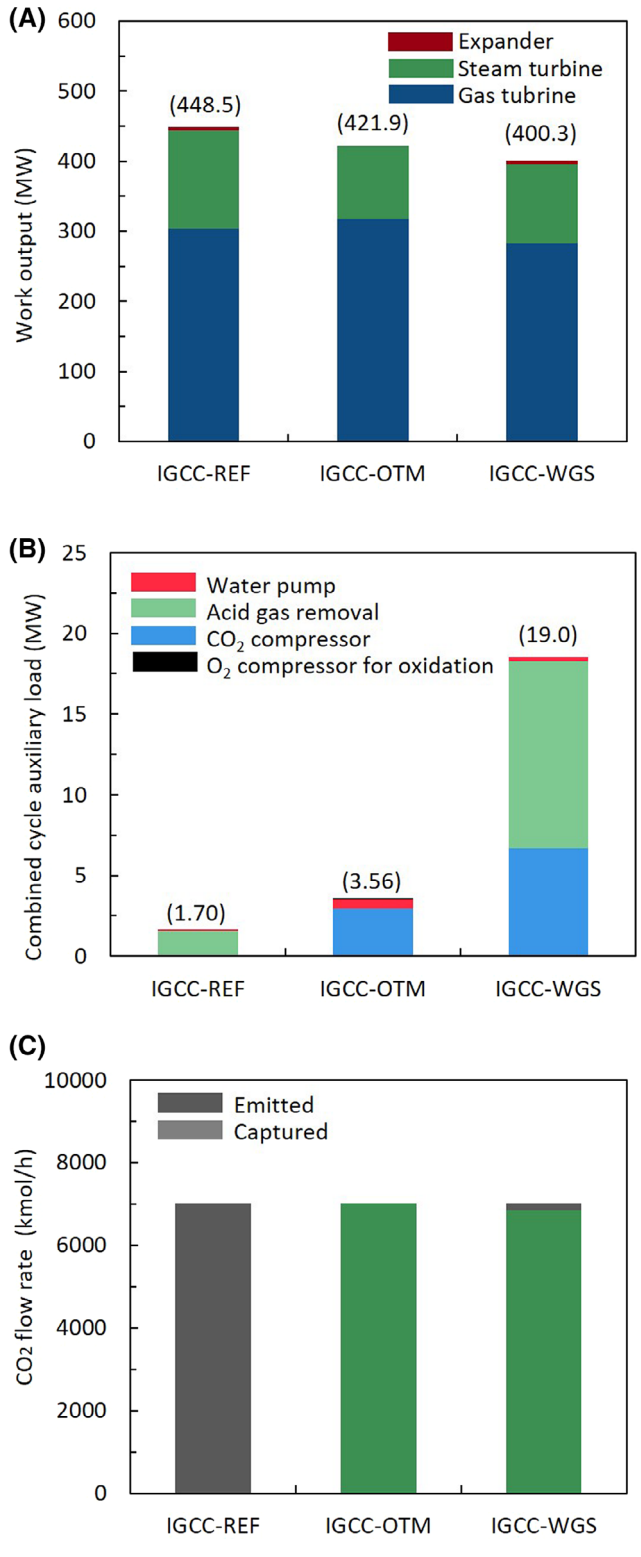

FIGURE 5 The comparison of A, the work output, B, the combined cycle auxiliary loads (absolute values), and C, CO_2 flow rates for the emitted and captured streams of the three IGCC systems with 1000 MW input. The number in the brackets are the sums of corresponding bars

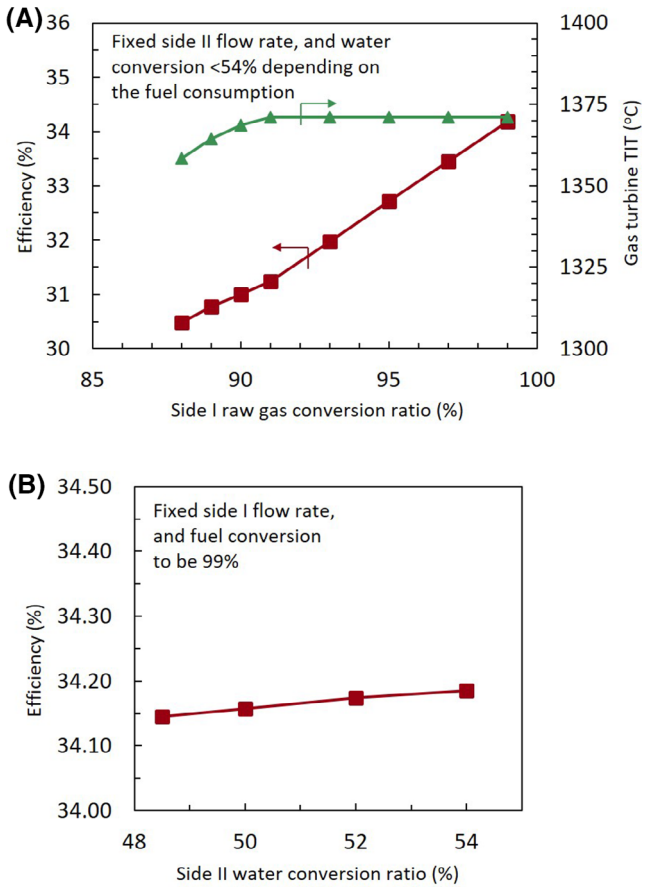

FIGURE 6 The dependence of system efficiency on the conversion of A, raw gas on side I and B, that of water on side II. It also shows the gas turbine TIT drops to lower than 1371°C in A

When the operating temperature drops from 1000 to 825°C, the system efficiency is reduced slightly. This is due to the decrease of H_2O conversion ratio and the heat integration between high temperature syngas products and lower temperature membrane reactors. On the one hand, higher operating temperature favors the operation due to higher hydrogen production rates,[18] and hence, smaller membrane surface areas are required for the same hydrogen output. On the other hand, the syngas temperature at the outlet of the radiant cooler increases with membrane temperatures, as shown in Figure 7B. This means the gas cleaning system or the dust collector should operate at higher temperatures, which might not be possible based on current gas filtering technologies.[35] Furthermore, when the operating temperature is lower than 825°C, it is difficult to achieve isothermal operation while keeping the MITA > 20°C (or >10°C in HRSG) in the heat exchangers. Therefore, the optimum temperature for the membrane reactor should be around 850°C.

5.3 | Pressure drop dependence

The pressure drop and compensation in both the feed and sweep sides is an energy penalty in the membrane

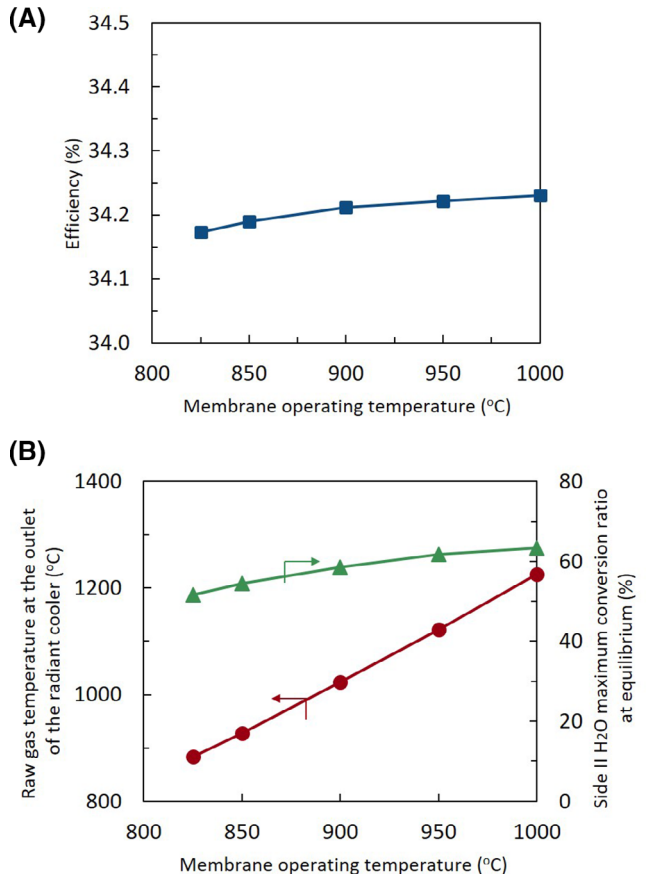

FIGURE 7 The dependence of A, system efficiency and B, raw gas temperature at the outlet of the radiant cooler and the maximum H_2O conversion ratio on side II on the operating temperature of the membrane reactor

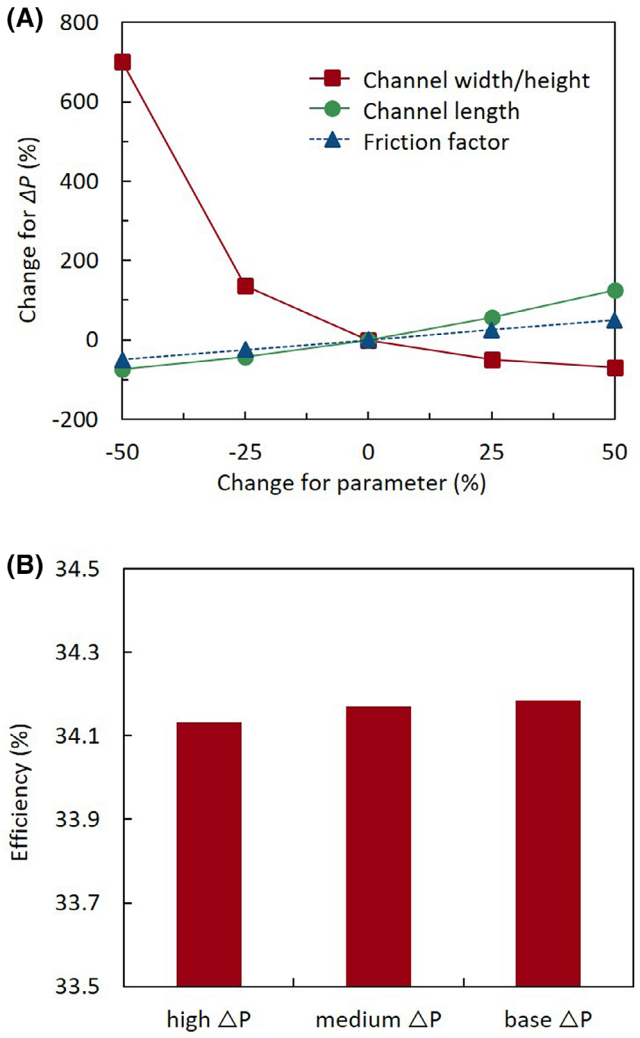

FIGURE 8 A, Sensitivity of the pressure drop to the channel width/height, channel length, and friction factor. B, The system efficiency decreases with increasing pressure drop (high $\Delta P = 1$ bar and medium $\Delta P = 0.5$ bar for both feed and sweep sides)

reactor. The membrane reactor configuration (eg, planar, tubular, or monolith membrane reactor), feed and sweep gas flow rates, operating temperatures and pressures all impact the pressure drop in the reactor. In this study, we use a simplified square-shape monolith membrane reactor as an example to estimate the pressure drop based on the correlation of flow in a smooth pipe.[43]

$$\text{For laminar flow:} \quad f = \frac{57}{\mathrm{Re}_{D_h}} \tag{4}$$

$$\text{For turbulent flow:} \quad f = \left(0.79 \ln \mathrm{Re}_{D_h} - 1.64\right)^{-2} \tag{5}$$

Here f is the friction factor, (dimensionless), Re is the Reynolds number, (dimensionless), and D_h is the hydraulic diameter, (m). The dimensions of the membrane reactor is $W \times H \times L = 1\ \text{cm} \times 1\ \text{cm} \times 2\ \text{m}$, similar to the monolith membrane reactor used for oxygen production,[44,45] monolith reformer,[46,47] and solid oxide electrolysis cells.[48,49] Details on the pressure drop evaluation can be found in Supporting Information.

The smooth pipe assumption can be relaxed, and the actual design of the membrane can be different. Therefore, sensitivity analysis is used to determine how the reactor parameters, such as the channel width/height, channel length, and the friction factor impact the pressure drop. The sensitivity of metric b to a parameter a is calculated as:

$$S_{a-b} = \frac{\partial \ln b}{\partial \ln a} \approx \frac{a}{b} \frac{\Delta b}{\Delta a} \tag{6}$$

where a is parameter and b is the metric for which the sensitivity is calculated. We change the parameters by ±25% and ± 50%, and evaluate the sensitivity of the pressure drop. Results are shown in the Figure 8A. The channel width/height affects the pressure drop the most, while the channel and friction factor have similar impacts on the pressure drop. This again confirm that

although the assumption of a smooth surface underestimate the pressure drop, its impact is not as important as varying the channel sizes.

The pressure drop evaluated using monolith reactor with wide smooth channels is almost negligible (11 Pa for feed side and 6.5 Pa for sweep side) due to small flow rates and large channel width/height. Previous studies also showed the pressure drop in monolith membrane reactors decreases greatly at larger channel width.[50] In this study, factors such as tube bending and reactor inlet/outlet effects are not considered, so the total pressure drop in the membrane reactor is underestimated. The pressure drop also depends strongly on the reactor design such as channel size and length. Therefore, we study the sensitivity of the system efficiency on the pressure drops (cases with high $\Delta P = 1$ bar and medium $\Delta P = 0.5$ bar for both feed and sweep sides are studied), shown in Figure 8B. Compared with the base case, the pressure drop in the membrane reactor change the system efficiency by −0.05% and −0.02% points for the high and medium pressure drop cases, respectively. Moreover, the pressure drop in the membrane reactor and the mass diffusion in the channel can both impact the conversion ratios along the membrane reactor, and therefore, affect the oxygen flux. Thus, higher fidelity models should be developed to optimize the membrane reactor design.

6 | CONCLUSIONS

In this article, we studied a novel IGCC technology with CC using an OTM reactor, IGCC-OTM. The sensitivity of the system efficiency to the operating parameters such as temperatures, pressure drops, and gas conversion ratios is also investigated. Results are as follows:

1 The IGCC-OTM (100% CC) system efficiency is only 3.2%-point lower than the same IGCC system without CC, which is much better than the 6.8%-point penalty in IGCC-WGS with 97% CC. The IGCC-OTM system also reduces the auxiliary power consumption associated with CO_2 separation and compression by 81% as compared with IGCC-WGS. Besides, the SPECCA of the IGCC-OTM is only 1.08 MJ $kgCO_2^{-1}$, which is 59% lower than that of the IGCC-WGS.
2 The gas conversion ratio of the syngas has higher impact on the system efficiency than that of the water splitting ratio. When the syngas conversion decreases from 99% to 88%, the IGCC-OTM efficiency drops from 34.2% to 30.5%. Although water splitting ratio has very small impacts on the system efficiency, it should be maintained higher than 48% to limit the dilution in the hydrogen fuel and achieve the TIT to be 1371°C under current system configuration.
3 Higher OTM operating temperatures lead to higher system efficiency due to the better utilization of the thermal energy in the high temperature gasifier products and higher water conversion ratios. However, higher OTM temperature also raises the operating temperature in the solid filter upstream, which could be undesirable for the filter system.
4 The sensitivity of the pressure drop in the membrane reactor is quantified. The channel width/height has the largest impact on the pressure drop, followed by the channel length and the friction factor. Higher pressure drop in the OTM reactor leads to lower efficiency, with −0.05% point difference when the pressure drop is 1 bar compared with the base of negligible pressure drop.

ACKNOWLEDGMENTS

Xiao-Yu Wu and Ahmed F. Ghoniem would like to thank Exelon Corporation for the funding. Aspen Plus was generously provided by Aspen Technology. Lili Cai, Xuefeng Zhu, and Weishen Yang would like to thank the National Natural Science Foundation of China (21776267), grants of Dalian National Laboratory for Clean Energy (DNL) (DNL180203), the Liaoning Revitalization Talents Program (XLYC1801004), and the Youth Innovation Promotion Association of the Chinese Academy of Sciences (Y201829).

ORCID

Xuefeng Zhu https://orcid.org/0000-0001-5932-7620

REFERENCES

[1] International Energy Agency, Coal 2018: analysis and forecasts to 2023. https://www.iea.org/coal2018/ (accessed: July 2019).
[2] P. Patrizio, S. Leduc, F. Kraxner, S. Fuss, G. Kindermann, S. Mesfun, K. Spokas, A. Mendoza, N. Mac Dowell, E. Wetterlund, J. Lundgren, E. Dotzauer, P. Yowargana, M. Obersteiner, *Joule.* **2018**, *2*(12), 2633. https://doi.org/10.1016/j.joule.2018.10.004.
[3] B. R. Sutherland, *Joule.* **2019**, *3*(2), 319. https://doi.org/10.1016/j.joule.2019.01.015.
[4] World Energy Council, World Energy Trilemma Index. **2019**. https://www.worldenergy.org/assets/downloads/WETrilemma_2019_Full_Report_v4_pages.pdf (accessed: February 2020).
[5] World Coal Association. Coal and the sustainable development goals roundtable summary. https://www.worldcoal.org/sites/default/files/Coal and the SDGs London roundtable—summary.pdf (accessed: July **2019**).
[6] A. F. Ghoniem, *Prog. Energy Combust. Sci.* **2011**, *37*(1), 15. https://doi.org/10.1016/j.pecs.2010.02.006.
[7] D. Y. C. Leung, G. Caramanna, M. M. Maroto-Valer, *Renew. Sustain. Energy Rev.* **2014**, *39*, 426. https://doi.org/10.1016/j.rser.2014.07.093.
[8] T. F. Wall, *Proc. Combust. Inst.* **2007**, *31*(1), 31. https://doi.org/10.1016/j.proci.2006.08.123.
[9] C. Descamps, C. Bouallou, M. Kanniche, *Energy.* **2008**, *33*(6), 874. https://doi.org/10.1016/j.energy.2007.07.013.

[10] M. Gazzani, E. Macchi, G. Manzolini, *Int. J. Greenh Gas Control.* **2013**, *12*, 493. https://doi.org/10.1016/j.ijggc.2012.06.010.
[11] C. Ortiz, J. M. Valverde, R. Chacartegui, *Energy Technol.* **2016**, *4*(10), 1317. https://doi.org/10.1002/ente.201600390.
[12] S. Hoffmann, M. Bartlett, M. Finkenrath, A. Evulet, T. P. Ursin, *J. Eng. Gas Turbines Power* **2008**, *131*(2), 021701. https://doi.org/10.1115/1.2982147.
[13] D. Jansen, M. Gazzani, G. Manzolini, E. van Dijk, M. Carbo, *Int. J. Greenh Gas Control.* **2015**, *40*, 167. https://doi.org/10.1016/j.ijggc.2015.05.028.
[14] R. M. Cuéllar-Franca, A. Azapagic, *J CO2 Util.* **2015**, *9*, 82. https://doi.org/10.1016/j.jcou.2014.12.001.
[15] J. Tonziello, M. Vellini, *Energy Procedia.* **2011**, *4*, 637. https://doi.org/10.1016/j.egypro.2011.01.099.
[16] M. Gazzani, D. M. Turi, A. F. Ghoniem, E. Macchi, G. Manzolini, *Int. J. Greenh Gas Control.* **2014**, *25*, 62. https://doi.org/10.1016/j.ijggc.2014.03.011.
[17] S. R. Venna, M. A. Carreon, *Chem. Eng. Sci.* **2015**, *124*, 3. https://doi.org/10.1016/j.ces.2014.10.007.
[18] L. Cai, X.-Y. Wu, X. Zhu, A. F. Ghoniem, W. Yang, *AIChE J.* **2020**, *66*, e16247. https://doi.org/10.1002/aic.16247.
[19] L. Cai, S. Hu, Z. Cao, H. Li, X. Zhu, W. Yang, *AIChE J.* **2019**, *65*(3), 1088. https://doi.org/10.1002/aic.16491.
[20] C. Zhang, J. Sunarso, S. Liu, *Chem. Soc. Rev.* **2017**, *46*(10), 2941. https://doi.org/10.1039/C6CS00841K.
[21] M. Tou, R. Michalsky, A. Steinfeld, *Joule.* **2017**, *1*(1), 146. https://doi.org/10.1016/j.joule.2017.07.015.
[22] X.-Y. Wu, A. F. Ghoniem, *Prog. Energy Combust. Sci.* **2019**, *74*, 1. https://doi.org/10.1016/J.PECS.2019.04.003.
[23] W. Li, Z. Cao, L. Cai, L. Zhang, X. Zhu, W. Yang, *Energy Environ. Sci.* **2017**, *10*(1), 101. https://doi.org/10.1039/C6EE02967A.
[24] X. Y. Wu, A. F. Ghoniem, M. Uddi, *AIChE J.* **2016**, *62*(12), 4427. https://doi.org/10.1002/aic.15518.
[25] X. Zhu, W. Yang, *Adv. Mater.* **2019**, *31*, 1902547. https://doi.org/10.1002/adma.201902547.
[26] Kriegel R. Energy demand of oxygen membrane plants. https://www.ikts.fraunhofer.de/content/dam/ikts/abteilungen/umwelt_und_verfahrenstechnik/hochtemperaturseparation_und_katalyse/hochtemperaturmembranen_und_speicher/energiebedarf_sauerstoff-membrananlage/2013_IKTS_energy_demand_o2_membrane_plants.pdf. Published 2014. (accessed: April **2019**).
[27] R. P. Field, R. Brasington, *Ind. Eng. Chem. Res.* **2011**, *50*(19), 11306. https://doi.org/10.1021/ie200288u.
[28] K. Gerdes, J. Black, J. Haslback, A. P. Jones, W. Lundberg, V. Shah, A. Kyle, E. Lewis, Cost and performance of PC and IGCC plants for a range of carbon dioxide capture, US DOE Report. **2013**.
[29] H. H. W. Funke, N. Beckmann, S. Abanteriba, *Int. J. Hydrogen Energy.* **2019**, *44*(13), 6978. https://doi.org/10.1016/j.ijhydene.2019.01.161.
[30] Goldmeer J. Power to gas: hydrogen for power generation, GE power. https://www.ge.com/content/dam/gepower/global/en_US/documents/fuel-flexibility/GEA33861 power to gas—hydrogen for power generation.pdf. (accessed: December **2019**).
[31] Gas tubines of mitsubishi hitachi power systems. http://www.mhps.com/products/gasturbines/ (accessed: April **2020**).
[32] S. Chen, N. Lior, W. Xiang, *Appl. Energy* **2015**, *146*, 298. https://doi.org/10.1016/j.apenergy.2015.01.100.
[33] X. Zhang, *Clean Energy* **2018**, *2*(2), 126. https://doi.org/10.1093/ce/zky012.
[34] Z. Kapetaki, P. Brandani, S. Brandani, H. Ahn, *Int. J. Greenh Gas Control.* **2015**, *39*, 17. https://doi.org/10.1016/j.ijggc.2015.04.015.
[35] S. Heidenreich, *Fuel.* **2013**, *104*, 83. https://doi.org/10.1016/j.fuel.2012.07.059.
[36] J.-H. Wang, M. Liu, *J. Power Sources.* **2008**, *176*(1), 23. https://doi.org/10.1016/j.jpowsour.2007.10.025.
[37] C. Duan, R. J. Kee, H. Zhu, C. Karakaya, Y. Chen, S. Ricote, A. Jarry, E. J. Crumlin, D. Hook, R. Braun, N. P. Sullivan, R. O'Hayre, *Nature* **2018**, *557*(7704), 217. https://doi.org/10.1038/s41586-018-0082-6.
[38] L. Yang, S. Wang, K. Blinn, M. Liu, Z. Liu, Z. Cheng, M. Liu, *Science.* **2009**, *326*(5949), 126. https://doi.org/10.1126/science.1174811.
[39] P. Ahmed, M. A. Habib, R. Ben-Mansour, P. Kirchen, A. F. Ghoniem, *Energy.* **2014**, *77*, 932. https://doi.org/10.1016/j.energy.2014.10.003.
[40] D. M. Turi, P. Chiesa, E. Macchi, A. F. Ghoniem, *Energy.* **2016**, *96*, 127. https://doi.org/10.1016/j.energy.2015.12.055.
[41] Goodwin D, Malaya N, Moffat H, Speth R. Cantera: an object-oriented software toolkit for chemical kinetics, thermodynamics, and transport processes. https://code.google.com/p/cantera/. (accessed: **2013**).
[42] Smith GP, Golden DM, Frenklach M, Moriarty NW, Eiteneer B, Goldenberg M, Bowman CT, Hanson RK, Song S, Gardiner WC, Jr., Lissianski VV, Qin Z. GRI-Mech 3.0. http://www.me.berkeley.edu/gri_mech/ (accessed: **2019**).
[43] A. F. Mills, *Heat Transfer*, Richard D. Irwin, Inc., Boston, MA **1992**.
[44] M. A. Nemitallah, M. A. Habib, R. Ben-mansour, A. F. Ghoniem, *J. Membr. Sci.* **2014**, *450*, 60. https://doi.org/10.1016/j.memsci.2013.08.040.
[45] K. Eichhorn Colombo, V. V. Kharton, O. Bolland, *Energy & Fuels.* **2010**, *24*(1), 590. https://doi.org/10.1021/ef9004253.
[46] Z. Zhao, C. O. Iloeje, T. Chen, A. F. Ghoniem, *Fuel.* **2014**, *121*, 327. https://doi.org/10.1016/j.fuel.2013.11.056.
[47] E. J. Sheu, A. F. Ghoniem, *Sol. Energy.* **2016**, *125*, 339. https://doi.org/10.1016/j.solener.2015.12.024.
[48] C. Bao, N. Cai, E. Croiset, *J. Power Sources* **2011**, *196*(20), 8424. https://doi.org/10.1016/j.jpowsour.2011.05.032.
[49] H. J. Hwang, J.-W. Moon, S. Lee, E. A. Lee, *J. Power Sources* **2005**, *145*(2), 243. https://doi.org/10.1016/j.jpowsour.2005.02.063.
[50] N. D. Mancini, A. Mitsos, *Energy* **2011**, *36*(8), 4721. https://doi.org/10.1016/j.energy.2011.05.024.

SUPPORTING INFORMATION

Additional supporting information may be found online in the Supporting Information section at the end of this article.

How to cite this article: Wu X-Y, Cai L, Zhu X, Ghoniem AF, Yang W. A high-efficiency novel IGCC-OTM carbon capture power plant design. *Journal of Advanced Manufacturing and Processing*. 2020;2:e10059. https://doi.org/10.1002/amp2.10059